



KTH Engineering Sciences

Computational methods for microfluidics

LUDVIG AF KLINTEBERG

Licentiate Thesis in Applied and Computational Mathematics
Stockholm, Sweden 2013

TRITA-NA 2013:01
ISSN 0348-2952
ISRN KTH/NA--13/01--SE
ISBN 978-91-7501-625-2

KTH School of Engineering Sciences
SE-100 44 Stockholm
SWEDEN

Akademisk avhandling som med tillstånd av Kungl Tekniska högskolan framlägges till offentlig granskning för avläggande av teknologie licentiatexamen i tillämpad matematik och beräkningsmatematik med inriktning mot numerisk analys tisdagen den 19:e februari 2013 klockan 10.00 i sal F3, Lindstedtsvägen 26, KTH, Stockholm.

© Ludvig af Klinteberg, januari 2013

Tryck: E-print AB, 2013

Abstract

This thesis is concerned with computational methods for fluid flows on the microscale, also known as microfluidics. This is motivated by current research in biological physics and miniaturization technology, where there is a need to understand complex flows involving microscale structures. Numerical simulations are an important tool for doing this.

The first paper of the thesis presents a numerical method for simulating multiphase flows involving insoluble surfactants and moving contact lines. The method is based on an explicit interface tracking method, wherein the interface between two fluids is decomposed into segments, which are represented locally on an Eulerian grid. The framework of this method provides a natural setting for solving the advection-diffusion equation governing the surfactant concentration on the interface. Open interfaces and moving contact lines are also incorporated into the method in a natural way, though we show that care must be taken when regularizing interface forces to the grid near the boundary of the computational domain.

In the second paper we present a boundary integral formulation for sedimenting particles in periodic Stokes flow, using the completed double layer boundary integral formulation. The long-range nature of the particle-particle interactions lead to the formulation containing sums which are not absolutely convergent if computed directly. This is solved by applying the method of Ewald summation, which in turn is computed in a fast manner by using the FFT-based spectral Ewald method. The complexity of the resulting method is $\mathcal{O}(N \log N)$, as the system size is scaled up with the number of discretization points N . We apply the method to systems of sedimenting spheroids, which are discretized using the Nyström method and a basic quadrature rule.

The Ewald summation method used in the boundary integral method of the second paper requires a decomposition of the potential being summed. In the introductory chapters of the thesis we present an overview of the available methods for creating Ewald decompositions, and show how the methods and decompositions can be related to each other.

Preface

This thesis consists of an introduction and two papers. The included papers are:

Paper I

L. af Klinteberg, D. Lindbo, and A.-K. Tornberg. An explicit Eulerian method for multiphase flow with contact line dynamics and insoluble surfactant, *Preprint*, 2012.

The author of this thesis contributed to the ideas, methods and their implementations, performed the numerical computations and drafted a portion of the manuscript.

Paper II

L. af Klinteberg and A.-K. Tornberg. Fast Ewald summation for periodic suspensions using completed double layer boundary integral method, *Preprint*, 2013.

The author of this thesis contributed to the ideas and methods, implemented the methods, performed the numerical computations and drafted the manuscript.

Contents

Contents	vii
1 Introduction	1
1.1 Microfluidics	2
1.2 Overview of this thesis	2
2 Multiphase flow, surfactants and wetting	5
2.1 Multiphase flow	5
2.2 Surfactants	8
2.3 Wetting	9
2.4 Simulating wetting flows with surfactants	9
3 Stokes flow and periodic suspensions	11
3.1 Boundary integral formulation	11
3.2 Sedimentation in suspensions	13
3.3 Periodic double layer formulation	14
4 Ewald summation	17
4.1 Stresslet decomposition	18
4.2 Truncation error estimates	19
4.3 Fast Ewald summation	21
5 Ewald decompositions	23
5.1 Splitting and screening	23
5.2 Summary of decompositions	26
6 Conclusions and future work	29
Bibliography	31

Chapter 1

Introduction

Fluids, meaning gases and liquids, are a central part of the world we live in. The wind and rain outside the window, the air we breathe and the blood flowing in our veins are all governed by the same physical laws. The subject of fluid mechanics studies how fluids behave in different situations, and it is centered around the Navier-Stokes equations for incompressible flow of Newtonian fluids,

$$\begin{aligned}\rho \left(\frac{\partial \mathbf{u}}{\partial t} + (\mathbf{u} \cdot \nabla) \mathbf{u} \right) &= -\nabla P + \mu \nabla^2 \mathbf{u} + \mathbf{f}, \\ \nabla \cdot \mathbf{u} &= 0,\end{aligned}\tag{1.1}$$

which describe almost all of the fluid phenomena we see around us¹. This set of partial differential equations (PDEs) is nonlinear and very challenging to work with. Real world problems, such as the question of how the air flows around (and lifts!) an airplane or how the water flows around a ship hull, can not be solved by purely theoretical considerations. Before the advent of computers, engineers and scientists had to rely solely on experimental work in wind tunnels and towing tanks if they wanted to analyze these flows. In the 1960's the first computer simulations of fluid flows were performed, and the last half-century has seen a massive development of both computer power and numerical methods. Today we can play computer games with real-time smoke effects, and we regularly expect the weather simulations of our meteorological institutes to predict the flow patterns of the sky more than a week into the future. Scientists and engineers are now abandoning their wind tunnels in favor of computer simulations, which offer cheap and accurate results without even having to get your hands dirty.

¹Some flows require the general form of the Navier-Stokes equations, for example ketchup flow (non-Newtonian liquid) and the airflow around a supersonic fighter jet (compressible flow).

1.1 Microfluidics

The field of microfluidics deals with fluid flows at the micrometer scale. It has grown continuously since the 1990's, motivated by questions arising from biological physics and advances in miniaturization technology, especially in what is referred to as lab-on-a-chip devices (see for example Tabeling [53] and Stone [52] for a thorough introduction to the subject). The idea of these devices is to take all the steps of a certain laboratory process, miniaturize them and put them together on one chip. A typical blood sample analysis, where one wants to detect whether a certain protein or hormone is present in a patients blood, can for example be miniaturized, thereby reducing the required sample volume to a nano- or picoliter, and at the same time speeding up the analysis time. One could potentially construct a device which splits a single drop of blood into a thousand small droplets and performs a different analysis on each droplet, giving a doctor an immediate overview of a patients health.

At the small length scales considered in microfluidics, effects related to fluid viscosity — like the upstream buckling we observe when pouring syrup on pancakes — start to dominate over the inertia effects that we are used to observing around us — like the chaotic sloshing which we associate with rapidly moving a mug full of coffee. At the same time, effects related to surfaces and fluid interfaces become more pronounced as the surface-to-volume ratio increases. As an example, consider a box with sides L , filled with a liquid. The surface-to-volume ratio of such a box is $6:L$. In the case of the box being a large tank with side $L = 6$ m the ratio would be 1:1, while in the case of the box being a miniature container with side one micrometer, $L = 10^{-6}$ m, the ratio would be 6000000:1. One can then easily understand that flow effects related to physics happening at the inner surfaces of the box would have a much larger relative importance in the miniature case. As these surface effects become increasingly important as we scale down our problems, so does the need to accurately model and capture them in numerical simulations.

1.2 Overview of this thesis

In chapter 2 of this thesis we discuss a method for accurately simulating multiphase flows, which are fluid flows containing interfaces between gases and liquids, such as drops and bubbles, or between immiscible liquids, such as oil and water. We show how the method can be used to handle flow problems where there are surface tension altering chemicals present on the surface, and further extend it to handle wetting problems, where we have a drop attached to a wall.

We turn our attention to a different field of microfluidics in chapter 3, where we discuss a method for simulating large systems of particles moving in a very viscous liquid, for which a simplification of the Navier-Stokes equations (1.1) is valid. The method can be used for the study of particle suspensions, to understand both how the particles affect the macroscopic flow properties of the suspension, and the fashion in which the particles settle if the fluid is left resting. The method is

based on discretization of a boundary integral equation, the solution of which is accelerated by an Ewald summation method, described in chapter 4. In chapter 5 we continue discussing Ewald summation. We give an overview of the available methods for creating the decompositions used in Ewald summation, and show how the methods and decompositions can be related to each other.

Chapter 2

Multiphase flow, surfactants and wetting

Multiphase flow refers to flow situations including two (or more) fluids, which are separated by an interface. Examples of such interfaces are the surfaces of ink drops in an inkjet printer and gas bubbles in boiling water, and the surfaces separating oil from water in an emulsion, such as milk or mayonnaise. We will here not make the distinction between *multiphase* (one fluid in different phases) and *multicomponent* (different fluids) flows, but rather just consider systems where the fluids involved are immiscible and there is no phase change taking place.

In microfluidic applications, and particularly in lab-on-a-chip devices, multiphase flows are commonplace. Drops are often used as atomic units of fluid for analysis or chemical reactions, and it is therefore important to understand and be able to control how drops form, coalesce, move and break up as they move through the device [52, 62]. However, surface tension and wall effects are dominant at the scales in question, due to the large surface-to-volume effects. This makes the fluids behave quite differently from what we are used to observing on the macroscale, which is why numerical simulations are an important tool for understanding and developing the flows in microfluidic devices.

In Paper I we present a method for two-phase flow with surfactants and contact line dynamics in two dimensions. Here we give an introduction to the concepts involved, as well as a brief overview of the available numerical methods.

2.1 Multiphase flow

Governing equations

For the setting of multiphase flow, we limit ourselves to two-dimensional flow, which is a valid simplification in many microfluidic applications. We consider the Navier-Stokes equations in non-dimensional form for the velocity and pressure fields \mathbf{u} and

P ,

$$\begin{aligned} \frac{\partial \mathbf{u}}{\partial t} + (\mathbf{u} \cdot \nabla) \mathbf{u} &= -\nabla P + \frac{1}{\text{Re}} \nabla^2 \mathbf{u} + \frac{1}{\text{ReCa}} \mathbf{f}, \\ \nabla \cdot \mathbf{u} &= 0. \end{aligned} \quad (2.1)$$

The Reynolds number $\text{Re} = \frac{\rho U L}{\mu}$ expresses the ratio of inertial to viscous forces for a liquid of density ρ and viscosity μ in a flow with characteristic length L and characteristic velocity U . The capillary number $\text{Ca} = \frac{\mu U}{\sigma}$ expresses the ratio of viscous to surface tension forces, where σ is the surface tension (or surface energy). The body forces of the system, represented by \mathbf{f} , are on the microscale completely dominated by the surface tension, so gravity can be neglected unless we are considering bubbles rising under buoyancy forces. The surface tension force can for a clean interface be expressed as [8],

$$\mathbf{f}(\mathbf{x}) = \begin{cases} \sigma \kappa \hat{\mathbf{n}}, & \mathbf{x} \in \Gamma, \\ 0, & \mathbf{x} \notin \Gamma, \end{cases} \quad (2.2)$$

where κ is the local curvature of the interface and $\hat{\mathbf{n}}$ is the normal vector. The interface Γ can in two dimensions naturally be viewed as a closed curve, which we parameterize in the arc length s . The time-dependence of the interface can then in Lagrangian form be expressed as an ODE,

$$\frac{d\Gamma(s)}{dt} = \mathbf{u}(\Gamma(s), t). \quad (2.3)$$

The velocity field $\mathbf{u}(\Gamma(s), t)$ is evaluated at the position of the interface and is governed by (2.1), which in turn is coupled to the interface through (2.2).

Numerical methods

The system which we describe in (2.1), (2.2) and (2.3) is seemingly simple, yet presents many computational difficulties. A large number of computational methods for multiphase flow have been developed since the beginning of the 1990's, all with the purpose of circumventing limitations of previous methods. There now exists a wide range of methods, all with different advantages. Which method is used in practice depends highly on the application at hand, and also on the availability of codes, since implementing a state-of-the-art method for multiphase flow is a demanding task. We here give a brief overview of some of the existing methods, and discuss the difference between explicit and implicit interface representations. For a more in-depth introduction to computational methods for multiphase flow, we refer to the recent review paper by Wörner [58].

Common to most multiphase methods for finite Reynolds number flows is that the flow field is computed on an Eulerian grid, either by solving the Navier-Stokes equations (2.1) or by using a lattice Boltzmann method [10], which solves a

mesoscale approximation of the Navier-Stokes equations. The task is then to solve the problem of tracking the interface Γ as it moves by (2.3), compute the surface tension force (2.2) on the interface and then evaluate the force on the grid. The essential difficulty in interface tracking is that the dimensionality of the interface is one less than the domain of the flow, meaning that the interface in practice never coincides with the Eulerian grid, if a fixed grid is used.

For zero Reynolds number flows, also known as Stokes flow or creeping flow, it is possible to use a boundary integral method instead of a grid-based method. This will be discussed further in chapter 3, though not in the setting of multiphase flow.

Explicit interface representation

In explicit interface tracking methods, the coordinates of the interface are explicitly tracked as the interface evolves. The most prominent of these methods is the front-tracking method [56, 57], where the interface is represented by a discrete set of marker points. These points need to be redistributed as the interface evolves, to maintain an accurate interpretation of the interface. This is relatively simple to implement in two dimensions, but more challenging in three dimensions, as the book keeping of the interface representation becomes more involved. The connection between the Lagrangian interface representation and the Eulerian grid is in the front-tracking method obtained by interpolation using regularized delta functions, which were introduced in the immersed boundary method by Peskin [36, 37].

A way of using an explicit interface tracking without having to interpolate between the interface and grid is to use a moving mesh method [17, 33, 43, 42], where the flow equations are solved on an unstructured grid, which is adapted to follow the interface at every time step. This allows the interface to be explicitly tracked, but requires efficient algorithms for automatically refining and coarsening the grid, especially in the case of large interface deformations.

A feature which is common to all explicit interface tracking methods is that one must explicitly treat topological changes to the interface, such as breakup and coalescence of drops. This requires extra modeling and additional implementation difficulties, but also allows for an accurate treatment of such phenomena, given a valid model.

Implicit interface representation

In implicit interface tracking methods, the location of the interface is not explicitly advected from one time step to another. Instead, the interface position is in each time step recovered from a scalar quantity, which is advected on an Eulerian grid. Such methods include volume of fluid [47], level set [48], conservative level set [34], phase field [3] and lattice Boltzmann [2].

Topological changes are handled automatically in all implicit interface tracking methods, although this behavior is not always physically motivated. The case

of coalescence appears to be particularly troublesome, as the so-called numerical coalescence creates results that differ from experiments [58].

2.2 Surfactants

Surfactants, or surface active agents, are molecules which adhere to the interfaces in multiphase flows, where they lower the surface tension. They occur in many systems, either by design (e.g. detergents), naturally (e.g. pulmonary surfactant [59]) or as contaminants, and can drastically affect the dynamics of drops and bubbles when present [51, 54]. Surfactants are classified as either soluble or insoluble, depending on if they can be present as a concentration both in the bulk fluid and on the interface, or just as a concentration on the interface. Insoluble surfactants can be modeled as a scalar concentration ρ , which is present on the interface Γ and governed by an advection-diffusion equation on the interface [50],

$$\frac{D\rho}{Dt} + \rho(\nabla_s \cdot \mathbf{u}) = \frac{1}{\text{Pe}_\Gamma} \nabla_s^2 \rho, \quad \mathbf{x} \in \Gamma, \quad (2.4)$$

where ∇_s is the surface gradient operator, which in two dimensions can be expressed as $\nabla_s = \hat{\boldsymbol{\tau}} \frac{d}{ds}$, and Pe_Γ is the Peclet number, governing surfactant diffusion on the interface. Soluble surfactants are also governed by an additional advection-diffusion equation in the domain, together with source terms linking the bulk concentration to the interface concentration [7].

The presence of a surfactant concentration $\rho(s)$ on the interface creates local variations in the surface tension σ . This can be modeled through the Langmuir equation of state [35], here stated in non-dimensional form,

$$\sigma(s) = 1 + E \ln(1 - \rho(s)),$$

where E is the dimensionless elasticity number, expressing to what extent surfactants modify the surface tension. This local variation in surface tension has a secondary effect; it generates a tangential force at the interface, proportional to the surfactant gradient on the surface. This force is known as the Marangoni stress, and it is central to many of the phenomena which are associated with surfactants. The full surface force at the interface is then

$$\mathbf{f} = \sigma \kappa \hat{\mathbf{n}} + \frac{E}{1 - \rho} \frac{d\rho}{ds} \hat{\boldsymbol{\tau}}, \quad \mathbf{x} \in \Gamma.$$

Simulating flows with surfactants involves representing the concentration ρ and solving (2.4) on the interface Γ , which is more natural in an explicit interface representation. There are however numerical methods for multiphase flows with surfactants using both explicit and implicit interface representations, and there has been much development in this area in recent years [1, 24, 29, 32, 55, 60].

2.3 Wetting

When the interface between two fluids comes into contact with a solid surface, there is a contact line (or point, in 2D), along which the three components meet. A simple example of a contact line is the intersection between glass, water and air that encircles a drop lying on a glass plate. The angle θ between the fluid-fluid interface and the solid is called the contact angle (see Figure 2.1). When the system is at rest, the surface energies $\sigma_1, \sigma_2, \sigma$ at the fluid-fluid and solid-fluid interfaces will be in horizontal equilibrium, which is formulated by Young's equation [12] for the static contact angle θ_s ,

$$\sigma_1 - \sigma_2 - \sigma \cos \theta_s = 0.$$

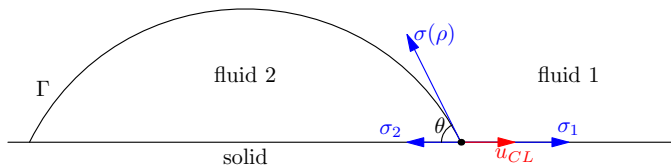


Figure 2.1: Drop wetting a solid surface, forming a contact angle θ between the surface and interface.

The case of dynamic wetting, when the contact line is moving on the solid with a velocity u_{CL} , is very common in many practical applications. However, it is also much more complicated than the static case. The Navier-Stokes equations with the standard no-slip boundary condition result in an infinite shear stress at the contact line, so additional modeling is required (see reviews by Blake [5] and Bonn et al. [6]). This makes numerical simulation of moving contact lines difficult, since one has to choose some kind of (more or less physical) model for the movement of the contact line. Nevertheless, simulations of wetting flows have been performed with good results, see for example Muradoglu & Tasoglu [31], Zahedi et al. [61] and Carlson et al. [9].

2.4 Simulating wetting flows with surfactants

In Paper I, we present a method for simulating two-phase flow with moving contact lines and insoluble surfactants in two dimensions. The method is based on an explicit interface tracking method developed by Khatri & Tornberg [24] and Lindbo & Tornberg [26, Paper V], where the interface is divided into segments, which are each represented by a function in a local coordinate frame (see Figure 2.2). This representation is natural for solving the surfactant PDE (2.4) on the interface, and also for representing open interfaces. To drive the motion of the contact line, we

apply a boundary condition derived by Ren & E [44], relating the contact line velocity u_{CL} to the contact angle θ . Figure 2.3 shows an example of the results.

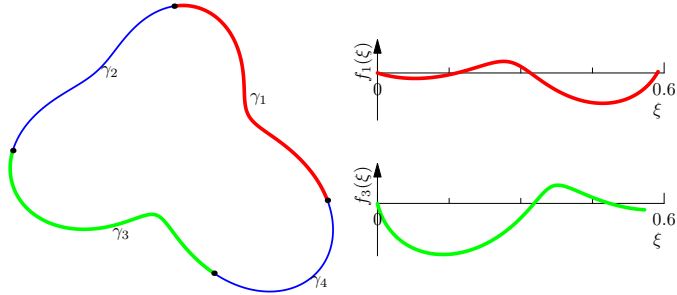


Figure 2.2: Interface (left), which is divided into segments. The segments are then represented in a local coordinate frame (right).

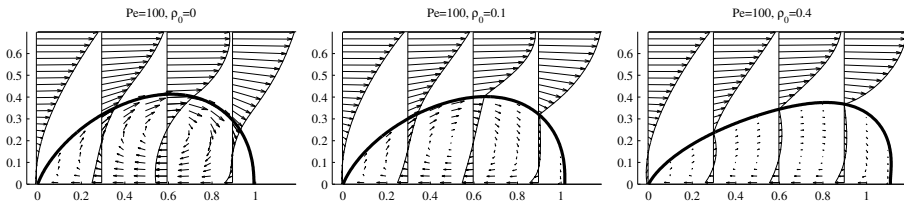


Figure 2.3: Drop on a solid surface in shear flow. To the left is a clean drop, with a velocity profile that is smooth across the interface. To the right is a drop with surfactants. The shear flow creates a surfactant gradient on the interface, resulting in Marangoni forces that cause a kink in the velocity profile across the interface.

Chapter 3

Stokes flow and periodic suspensions

Viscous forces are in many microfluidic applications dominant over the inertial forces, which are responsible for the onset of turbulence in flows on the macroscale. This is measured by the Reynolds number, $\text{Re} = \frac{\rho UL}{\mu}$, which describes the ratio of inertial to viscous forces for a liquid of density ρ and viscosity μ in a flow with characteristic length L and characteristic velocity U . For self-propelling microorganisms, such as swimming bacteria, the Reynolds number is on the order of 10^{-4} or 10^{-5} [41]. In such cases, when $\text{Re} \ll 1$, it is valid to linearize the Navier-Stokes equations (1.1) by assuming that $\text{Re} = 0$. The nonlinear convective term of the equations then disappears, and one obtains the linearized Stokes equations¹,

$$\begin{aligned} -\nabla P + \mu \nabla^2 \mathbf{u} + \mathbf{f} &= 0, \\ \nabla \cdot \mathbf{u} &= 0, \end{aligned} \tag{3.1}$$

where \mathbf{u} is velocity, P pressure and \mathbf{f} body force. The lack of time-dependence in (3.1) implies that the flow at any given time is completely determined by the boundary conditions, i.e. the flow has no "memory".

3.1 Boundary integral formulation

The benefit of working with the Stokes equations is that they belong to the class of linear PDEs with constant coefficients. This implies, by the Lorentz reciprocal theorem, that the flow in a domain can be expressed as a surface integral over the boundaries, assuming the boundaries Lyapunov smooth. This is beneficial because the dimensionality of the problem is reduced by one; instead of solving a problem in the entire domain we can solve a boundary integral representation of the problem on the surface, and then evaluate the solution in the domain.

¹We refer to Pozrikidis [39] for a complete version of the brief introduction to Stokes flow given here.

In the case of external flow we are concerned with the flow in the infinite domain D_e outside a body with surface Γ . The reciprocal theorem then states that for $\mathbf{x} \in D_e$, and given the velocity \mathbf{u} and force \mathbf{f} on Γ , then

$$\begin{aligned} u_j(\mathbf{x}) = & -\frac{1}{8\pi\mu} \int_{\Gamma} f_i(\mathbf{y}) G_{ij}(\mathbf{x}, \mathbf{y}) dS(\mathbf{y}) \\ & - \frac{1}{8\pi} \int_{\Gamma} u_i(\mathbf{y}) T_{ijk}(\mathbf{x}, \mathbf{y}) \hat{n}_k(\mathbf{y}) dS(\mathbf{y}), \end{aligned} \quad (3.2)$$

under the assumption that $|\mathbf{u}| = \mathcal{O}(|\mathbf{x}|^{-1})$ and $p = \mathcal{O}(|\mathbf{x}|^{-2})$ as $|\mathbf{x}| \rightarrow \infty$. The unit vector $\hat{\mathbf{n}}$ is the outward pointing normal. The kernels T and G are the stresslet and stokeslet fundamental singularities,

$$\begin{aligned} T_{ijk}(\mathbf{x}, \mathbf{y}) &= -6 \frac{r_i r_j r_k}{r^5}, \\ G_{ij}(\mathbf{x}, \mathbf{y}) &= \frac{\delta_{ij}}{r} + \frac{r_i r_j}{r^3}, \end{aligned} \quad (3.3)$$

where $\mathbf{r} = \mathbf{x} - \mathbf{y}$ and $r = |\mathbf{r}|$. The two integrals in the boundary integral representation (3.2) are called the single and double layer potentials, and both can be used independently to represent Stokes flow.

Keeping only the single layer potential and letting $\mathbf{x} \rightarrow \Gamma$, we obtain a weakly singular Fredholm equation of the first kind for an unknown single layer density \mathbf{f} , given a surface velocity \mathbf{u} ,

$$-\frac{1}{8\pi\mu} \int_{\Gamma} f_i(\mathbf{y}) G_{ij}(\mathbf{x}, \mathbf{y}) dS(\mathbf{y}) = \mathbf{u}(\mathbf{x}), \quad \mathbf{x} \in \Gamma. \quad (3.4)$$

The single layer formulation (3.4) is ill-conditioned, in the sense that the condition number is unbounded [18]. However, it is still usable for simulations, see [23, 21].

Keeping instead the double layer potential, we get the double layer representation for the velocity a point in the domain, such that for a double layer density \mathbf{q} on Γ ,

$$u_j(\mathbf{x}) = \int_{\Gamma} q_i(\mathbf{y}) T_{ijk}(\mathbf{x}, \mathbf{y}) \hat{n}_k(\mathbf{y}) dS(\mathbf{y}). \quad (3.5)$$

The actual values of \mathbf{q} depend on how we define the double layer representation, so we are free to scale it with a constant, as we have done here for convenience. Taking the limit $\mathbf{x} \rightarrow \Gamma$, the double layer potential contains a jump,

$$\lim_{\epsilon \rightarrow 0} u_j(\mathbf{x} \pm \epsilon \hat{\mathbf{n}}) = \mp 4\pi \mathbf{q}(\mathbf{x}) + \int_{\Gamma} q_i(\mathbf{y}) T_{ijk}(\mathbf{x}, \mathbf{y}) \hat{n}_k(\mathbf{y}) dS(\mathbf{y}). \quad (3.6)$$

This implies that given a surface velocity \mathbf{u} for the external surface, we get a weakly singular Fredholm equation of the second kind for an unknown density \mathbf{q} ,

$$u_j(\mathbf{x}) = -4\pi \mathbf{q}(\mathbf{x}) + \int_{\Gamma} q_i(\mathbf{y}) T_{ijk}(\mathbf{x}, \mathbf{y}) \hat{n}_k(\mathbf{y}) dS(\mathbf{y}), \quad \mathbf{x} \in \Gamma. \quad (3.7)$$

The singularity in the right hand side of (3.7) can be treated by the method of singularity subtraction, which reduces the order of the singularity (though it does not remove it completely, as we see in Paper II). One then applies the identity

$$\int_{\Gamma} T_{jlm}(\mathbf{x}, \mathbf{y}) \hat{n}_m(\mathbf{y}) dS(\mathbf{y}) = \delta_{jl} \begin{cases} 0, & \mathbf{x} \text{ outside } \Gamma, \\ 4\pi, & \mathbf{x} \in \Gamma, \\ 8\pi, & \mathbf{x} \text{ inside } \Gamma, \end{cases}$$

allowing us to restate (3.7) as

$$u_j(\mathbf{x}) = \int_{\Gamma} (q_i(\mathbf{y}) - q_i(\mathbf{x})) T_{ijk}(\mathbf{x}, \mathbf{y}) \hat{n}_k(\mathbf{y}) dS(\mathbf{y}), \quad \mathbf{x} \in \Gamma. \quad (3.8)$$

Working with (3.8), we can skip the term $\mathbf{y} = \mathbf{x}$ in numerical quadrature, since the integrand goes to zero as $\mathbf{y} \rightarrow \mathbf{x}$ (assuming \mathbf{q} smooth).

The benefit of the double layer formulation — compared to the single layer formulation — is that it is well-conditioned, in the sense that its condition number is bounded. The drawback is however that the double layer potential alone is incomplete, since it can only represent flows which have zero net force and torque on the surface Γ . There are various remedies for this, as discussed by Gonzalez [18]. We have used the completed double layer formulation of Power & Miranda [38], where two singular flow solutions (a stokeslet and a rotlet) located at an arbitrary point inside Γ are added to the double layer representation (3.5), to generate a completion flow that is able to represent net force and torque.

3.2 Sedimentation in suspensions

When a suspension of microparticles is left to rest, the particles will start to sediment due to gravity, unless they are neutrally buoyant. The sedimentation takes place on the microscale, yet it affects the macroscopic properties of the suspension. Understanding the sedimentation behavior of particles — and how it depends on their shape and volume fraction — is of value for scientists and engineers working with suspensions. It is also surprisingly difficult [19], and has been a field of active research for many years [11, 20].

Stokes equations (3.1) are in many cases valid when modeling sedimenting particles, due to the particles' small size and low individual velocities. However, the hydrodynamic interactions between the particles are long-range (decay as $1/r$), so in simulations a very large domain would be required to avoid boundary effects due to a finite-size domain. The remedy for this is to use periodic boundary conditions, where a primary cell is replicated infinitely in all directions. This means that one only considers particles in a box of dimensions $L_1 \times L_2 \times L_3$, and then requires the flow and pressure gradient fields to be periodic with respect to that box,

$$\begin{aligned} \mathbf{u}(\mathbf{x}) &= \mathbf{u}(\mathbf{x} + \boldsymbol{\tau}(\mathbf{p})), \\ \nabla P(\mathbf{x}) &= \nabla P(\mathbf{x} + \boldsymbol{\tau}(\mathbf{p})), \end{aligned}$$

where

$$\boldsymbol{\tau}(\mathbf{p}) = (p_1 L_1, p_2 L_2, p_3 L_3), \quad \mathbf{p} \in \mathbb{Z}^3.$$

When using a boundary integral method, this however means that the velocity at a point is determined by the integral over all particle surfaces all the way up to infinity. To make the evaluation of this infinite integral computationally attainable, a fast method is required. In molecular dynamics, the similar problem of computing an infinite sum of electrostatic potentials is solved by using fast Ewald summation methods, which are also applicable to the problem of periodic Stokes flow. In Paper II of this thesis, we present a method for simulating sedimenting spheroids of arbitrary aspect ratio, which is based on a periodic version of the double layer formulation (3.5) and accelerated by a fast Ewald method. We will give a brief review of the boundary integral formulation of this method in the remainder of this chapter, and discuss Ewald summation in chapter 4.

3.3 Periodic double layer formulation

We consider a primary cell with N_p rigid particles with surface Γ_α and center of mass $\mathbf{x}_c^{(\alpha)}$, $\alpha = 1, \dots, N_p$. Each particle is subject to an external (gravitational) force, $\mathbf{f}^{(\alpha)}$, and zero external torque. Introducing the periodic double layer potential on a surface Γ ,

$$\mathcal{W}_j[\Gamma, \mathbf{q}](\mathbf{x}) = \sum_{\mathbf{p} \in \mathbb{Z}^3} \int_{\Gamma} q_l(\mathbf{y}) T_{jlm}(\mathbf{x}, \mathbf{y} + \boldsymbol{\tau}(\mathbf{p})) \hat{n}_m(\mathbf{y}) dS(\mathbf{y}), \quad (3.9)$$

and the periodic stokeslet potential from a point force \mathbf{f} located at \mathbf{x}_c ,

$$\mathcal{V}_j[\Gamma, \mathbf{f}](\mathbf{x}) = \sum_{\mathbf{p} \in \mathbb{Z}^3} \frac{1}{8\pi\mu} G_{jlm}(\mathbf{x}, \mathbf{x}_c + \boldsymbol{\tau}(\mathbf{p})) f_m, \quad (3.10)$$

the periodic form of the completed double layer representation can be written

$$u_j(\mathbf{x}) = \sum_{\alpha=1}^{N_p} \left(\mathcal{W}_j[\Gamma_\alpha, \mathbf{q}](\mathbf{x}) + \mathcal{V}_j[\Gamma_\alpha, \mathbf{f}^{(\alpha)}](\mathbf{x}) \right). \quad (3.11)$$

The interpretation of this is that the flow at a point \mathbf{x} is influenced by all periodic images of all particles in the primary cell, and that the influence is long-range, since it decays as $1/r$. On the surface Γ_α of each particle we set a no-slip boundary condition. For a rigid body with center of mass $\mathbf{x}_c^{(\alpha)}$ and translational and rotational velocities $\mathbf{V}^{(\alpha)}$ and $\boldsymbol{\Omega}^{(\alpha)}$, this implies that

$$\mathbf{u}(\mathbf{x}) = \mathbf{U}^{(\alpha)}(\mathbf{x}) := \mathbf{V}^{(\alpha)} + \boldsymbol{\Omega}^{(\alpha)} \times (\mathbf{x} - \mathbf{x}_c^{(\alpha)}), \quad \mathbf{x} \in \Gamma_\alpha.$$

Now we let \mathbf{x} in (3.11) go to the surface Γ_β of one body, and apply the double layer jump (3.6) and the singularity subtraction (3.8). We then obtain the boundary integral formulation for the unknown density \mathbf{q} for our periodic system of sedimenting particles,

$$\sum_{\alpha=1}^{N_p} \left(\mathcal{W}_j[\Gamma_\alpha, \mathbf{q} - \mathbf{q}(\mathbf{x})](\mathbf{x}) + \mathcal{V}_j[\Gamma_\alpha, \mathbf{f}^{(\alpha)}](\mathbf{x}) \right) = U_j^{(\beta)}(\mathbf{x}), \quad (3.12)$$

$$\mathbf{x} \in \Gamma_\beta, \quad \beta = 1, \dots, N_p.$$

The system is closed by adding by the constitutive equations relating \mathbf{q} to $\mathbf{V}^{(\alpha)}$ and $\mathbf{\Omega}^{(\alpha)}$ [39],

$$\mathbf{V}^{(\alpha)} = -\frac{4\pi}{S_{\Gamma_\alpha}} \int_{\Gamma_\alpha} \mathbf{q}(\mathbf{y}) dS(\mathbf{y}),$$

$$\mathbf{\Omega}^{(\alpha)} = -4\pi \sum_{n=1}^3 \frac{\boldsymbol{\omega}^{(\alpha,n)}}{A_n^{(\alpha)}} \left(\boldsymbol{\omega}^{(\alpha,n)} \cdot \int_{\Gamma_\alpha} (\mathbf{y} - \mathbf{x}_c^{(\alpha)}) \times \mathbf{q}(\mathbf{y}) dS(\mathbf{y}) \right),$$

where S_{Γ_α} is the surface area of Γ_α and

$$A_n^{(\alpha)} = \int_{\Gamma_\alpha} \left[\boldsymbol{\omega}^{(\alpha,n)} \times (\mathbf{y} - \mathbf{x}_c^{(\alpha)}) \right] \cdot \left[\boldsymbol{\omega}^{(\alpha,n)} \times (\mathbf{y} - \mathbf{x}_c^{(\alpha)}) \right] dS(\mathbf{y}).$$

The vectors $\boldsymbol{\omega}^{(\alpha,n)}$, $n = 1, 2, 3$, are independent unit vectors, which must satisfy

$$\frac{1}{\sqrt{A_n^{(\alpha)} A_m^{(\alpha)}}} \int_{\Gamma_\alpha} \left[\boldsymbol{\omega}^{(\alpha,m)} \times (\mathbf{y} - \mathbf{x}_c^{(\alpha)}) \right] \cdot \left[\boldsymbol{\omega}^{(\alpha,n)} \times (\mathbf{y} - \mathbf{x}_c^{(\alpha)}) \right] dS(\mathbf{y}) = \delta_{mn}.$$

They can be quickly computed using the modified Gram-Schmidt (MGS) algorithm [13, p. 107].

To solve the system (3.12) numerically, we discretize the surface integrals using a Gaussian quadrature with weights w_j , such that for a function $g(\mathbf{x})$

$$\sum_{\alpha=1}^{N_p} \int_{\Gamma_\alpha} g(\mathbf{x}) dS(\mathbf{x}) \approx \sum_{\alpha,j} w_j^{(\alpha)} g(\mathbf{x}_j^{(\alpha)}) = \sum_{s=1}^N w_s g(\mathbf{x}_s), \quad (3.13)$$

where the sum $s = 1, \dots, N$ goes over all discretization points on all bodies in the primary cell. Applying the Nyström method, we then require the discrete version of (3.12) to be satisfied in every point,

$$-\sum_{\alpha=1}^{N_p} \mathcal{W}_j^h[\Gamma_\alpha, \mathbf{q} - \mathbf{q}(\mathbf{x}_t)](\mathbf{x}_t) + U_j(\mathbf{x}_t) = \sum_{\alpha=1}^{N_p} \mathcal{V}_j[\Gamma_\alpha, \mathbf{f}^{(\alpha)}](\mathbf{x}_t),$$

$$t = 1, \dots, N,$$

where \mathcal{W}^h is the double layer potential evaluated using the Gaussian quadrature (3.13). This is a full $3N \times 3N$ system which is non symmetric and well-conditioned, and therefore suitable for iterative solution using the GMRES algorithm [45]. Before that can be done however, a method for evaluating the infinite sums in (3.9) and (3.10) must be applied. This is where the subject of Ewald summation enters the picture, as we will see in the next chapter.

Chapter 4

Ewald summation

As we saw in the previous chapter, formulating a boundary integral equation for a periodic suspension of sedimenting particles in Stokes flow results in a system where each particle is influenced by all other particles, all the way up to infinity. From the discretization of the periodic double layer potential (3.9) we get an infinite sum of stresslet potentials¹

$$\begin{aligned} u_j^{(T)}(\mathbf{x}) &:= \sum_{\alpha=1}^{N_p} \mathcal{W}_j^h[\Gamma_\alpha, \mathbf{q}](\mathbf{x}) \\ &= \sum_{s=1}^N \sum_{\mathbf{p} \in \mathbb{Z}^3} T_{jlm}(\mathbf{x} - \mathbf{x}_s + \tau(\mathbf{p})) q_l(\mathbf{x}_s) n_m(\mathbf{x}_s), \end{aligned} \quad (4.1)$$

where $\mathbf{n}(\mathbf{x}_s) = w_s \hat{\mathbf{n}}(\mathbf{x}_s)$ is the discrete form of the vector surface element $d\mathbf{S}$, and the stresslet T is defined in (3.3). The sum over all periodic images \mathbf{p} has very slow decay, and furthermore it is only conditionally convergent, so direct evaluation of the sum is impractical. The standard remedy for this is to use Ewald summation, invented by P.P. Ewald [15] in 1921 for the computation of the electrostatic potential in periodic crystal lattices. The main idea behind the method is to decompose the periodic sum into two sums. One sum is designed to contain the singularity and converge rapidly, while the other is designed to be smooth, such that it converges rapidly in \mathbf{k} -space (Fourier space). In electrostatics, the potential $1/r$ is decomposed as

$$\frac{1}{r} = \frac{1}{r} - \frac{\operatorname{erfc}(\xi r)}{r} + \frac{\operatorname{erfc}(\xi r)}{r} = \frac{\operatorname{erf}(\xi r)}{r} + \frac{\operatorname{erfc}(\xi r)}{r}.$$

Figure 4.1 gives an illustration of how this works. The parameter ξ determines how

¹We will here only discuss the summation of the double layer potential. For the stokeslet potential the procedure is equivalent, though the details differ. We refer to Lindbo & Tornberg [27] for that.

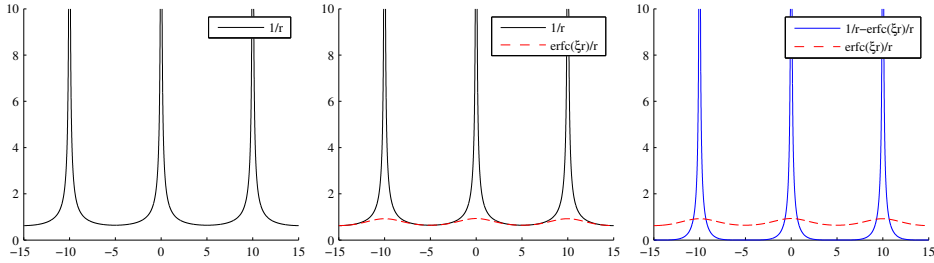


Figure 4.1: Illustration of how Ewald decomposition works. The original $1/r$ potential (left) is both long-range and singular. The long-range behavior is captured by the $\text{erf}(\xi r)/r$ component (middle), such that the final decomposition (right) separates it from the singular part.

fast the respective sums converge, and is used to balance the workload between them.

4.1 Stresslet decomposition

Ewald summation for the stresslet potential (4.1) builds on the same ideas as for the electrostatic potential, though the calculations are lengthier. An Ewald decomposition for the stresslet was first derived by Fan et al. [16], using the splitting method by Beenakker described in chapter 5. Recently, a second decomposition which appears to have better convergence properties was derived for the stresslet by Marin [30, Paper IV]. We here introduce the decomposition by Fan et al., where the periodic sum (4.1) is decomposed as

$$\begin{aligned}
 u_j^{(T)}(\mathbf{x}) &= \sum_{s=1}^N \sum_{\mathbf{p} \in \mathbb{Z}^3} A_{jlm}(\xi, \mathbf{x} - \mathbf{x}_s + \tau(\mathbf{p})) S_{lm}(\mathbf{x}_s) \\
 &+ \frac{1}{V} \sum_{\mathbf{k} \neq 0} B_{jlm}(\xi, \mathbf{k}) e^{-k^2/4\xi^2} \sum_{s=1}^N S_{lm}(\mathbf{x}_s) e^{-i\mathbf{k} \cdot (\mathbf{x} - \mathbf{x}_s)} \\
 &+ \frac{1}{V} \sum_{s=1}^N T_{jlm}^{(0)}(\mathbf{x}_s) S_{lm}(\mathbf{x}_s),
 \end{aligned} \tag{4.2}$$

where $S_{lm} := q_l n_m$ and $V = L_1 L_2 L_3$. The first sum in (4.2) converges rapidly in real space, with A defined as

$$\begin{aligned} A_{jlm}(\xi, \mathbf{r}) &:= C(\xi, \mathbf{r}) \hat{r}_j \hat{r}_l \hat{r}_m + D(\xi, \mathbf{r}) (\delta_{jl} \hat{r}_m + \delta_{lm} \hat{r}_j + \delta_{mj} \hat{r}_l), \\ C(\xi, \mathbf{r}) &= -\frac{2}{r} \left(\frac{3}{r} \operatorname{erfc}(\xi r) + \frac{2\xi}{\sqrt{\pi}} (3 + 2\xi^2 r^2 - 4\xi^4 r^4) e^{-\xi^2 r^2} \right), \\ D(\xi, \mathbf{r}) &= \frac{8\xi^3 r}{\sqrt{\pi}} (2 - \xi^2 r^2) e^{-\xi^2 r^2}. \end{aligned}$$

The second sum in (4.2) converges rapidly in \mathbf{k} -space, with B defined as

$$B_{jlm}(\xi, \mathbf{k}) := -i \frac{\pi}{k} \left[(\delta_{jl} \hat{k}_m + \delta_{lm} \hat{k}_j + \delta_{mj} \hat{k}_l) - 2\hat{k}_j \hat{k}_l \hat{k}_m \right] \left(8 + 2\frac{k^2}{\xi^2} + \frac{k^4}{\xi^4} \right).$$

The third sum in (4.2) is related to the $\mathbf{k} = 0$ term omitted from the \mathbf{k} -space sum, and is derived in Paper II for periodic sedimentation of rigid bodies. It turns out that the choice,

$$T_{jlm}^{(0)}(\mathbf{y}) = 8\pi \delta_{lm} y_j,$$

results in a zero mean flow through the primary cell, which is what we want if we are to observe particles sedimenting through a quiescent fluid.

4.2 Truncation error estimates

While the real- and \mathbf{k} -space sums in (4.2) are rapidly converging, they are still infinite. We therefore need to truncate them, and the question is when to do that. Ideally, we would like to keep only the terms required to compute $\mathbf{u}^{(T)}$ to a certain tolerance ϵ , and discard the rest. This is a question of delicate balancing; compute too few terms and we lose precision, compute too many and we do unnecessary work.

For the Ewald sum of the electrostatic potential, Kolafa & Perram [25] developed an RMS (root mean squares) error estimate for the case of charges randomly distributed in the primary cell. Their derivation builds on making a statistical estimate of the error, but is nevertheless highly predictive and widely used. In Paper II, we use the reasoning of Kolafa & Perram to develop truncation error estimates for the stresslet, when decomposed using the Ewald decomposition by Fan et al. The estimates are for the error in RMS, defined as

$$e_{rms,j} := \sqrt{\frac{1}{N} \sum_{s=1}^N (u_j(\mathbf{x}_s) - \tilde{u}_j(\mathbf{x}_s))^2},$$

where \mathbf{u} and $\tilde{\mathbf{u}}$ are the truncated and exact solutions, respectively. Both the real space and \mathbf{k} -space estimates contain a factor \sqrt{Q} , which depends on the system involved. We find that for randomly distributed point stresslets, we get very accurate

error estimates using the definition

$$Q := \sum_{s=1}^N \sum_{l=1}^3 \sum_{m=1}^3 q_l^2(\mathbf{x}_s) n_m^2(\mathbf{x}_s),$$

which sums the squared contributions from all the points. However, for the case of point sources related to quadrature of the double layer potential, using the above definition gives $Q \sim 1/N$ for a given geometry, with the number of discretization points increasing with N . In practice we find that Q is constant as the number of quadrature points is increased, so we redefine it as

$$Q := \left(\sum_{\alpha=1}^{N_p} S_{\Gamma_\alpha} \right) \left(\sum_{l=1}^3 \sum_{s=1}^N w_s q_l^2(\mathbf{x}_s) \right) \approx \sum_{\alpha=1}^{N_p} S_{\Gamma_\alpha} \sum_{l=1}^3 \|q_l\|_2^2,$$

where $\|\cdot\|_2$ is the 2-norm, defined as

$$\|f\|_2^2 = \sum_{\alpha=1}^{N_p} \int_{\Gamma_\alpha} f^2(\mathbf{y}) dS(\mathbf{y}).$$

Real space sum

In the real space sum the truncation is spatial, such that only points within a truncation radius r_c from the target point \mathbf{x} are included in the sum. For a given radius r_c and Ewald parameter ξ , the RMS error is estimated as

$$e_{rms}^{(R)} \approx e^{-\xi^2 r_c^2} \sqrt{\frac{1}{27} \frac{Q}{V} \xi^2 r_c (327 + 1588 \xi^2 r_c^2 - 1392 \xi^4 r_c^4 + 448 \xi^6 r_c^6)},$$

by following the steps of Kolafa & Perram.

k-space sum

In the \mathbf{k} -space sum, the truncation is on the reciprocal lattice, so we only compute the contribution from \mathbf{k} -vectors within a box K , such that $|k_i| \leq K$. Deriving an estimate for the \mathbf{k} -space truncation error turns out to be hard, but we heuristically find an error estimate that gives satisfactory results,

$$e_{rms}^{(F)} \approx e^{-K^2/4\xi^2 + 0.43K/\xi} \sqrt{\xi^2 L \frac{Q}{V}},$$

where $L = \min_i L_i$.

4.3 Fast Ewald summation

We have so far discussed how the slowly converging sum over periodic images (4.1) can be cast into an Ewald sum (4.2), which converges very fast. However, even though it is rapidly converging, the Ewald sum is very expensive to compute in practice, since it has $\mathcal{O}(N^2)$ complexity with a constant that grows rapidly with increasing r_c and K . This complexity can be reduced to $\mathcal{O}(N \log N)$ by applying a mesh-based method, which allows the \mathbf{k} -space sum to be computed using a fast Fourier transform (FFT). Such methods include the particle–particle–particle–mesh (P³M), particle mesh Ewald (PME) and smooth particle mesh Ewald (SPME), all of which are introduced in a unified way by Deserno & Holm [14]. A recent contribution to this class of methods is the spectral Ewald (SE) method by Lindbo & Tornberg [27, 28], which uses scaled Gaussians instead of interpolation polynomials to create a grid representation of the pointwise charge density. This decouples the approximation error of the summation method from the truncation error of the Ewald sum, thus reducing the memory requirements of the method by allowing a minimal FFT grid to be used.

These mesh based fast Ewald methods are widely used for computing the long-range interactions in molecular simulations, but they have also been applied to hydrodynamic problems with Stokes flow. The PME method was used by Sierou & Brady [49] for their accelerated Stokesian dynamics (ASD), simulating suspensions containing up to 1000 spheres. Saintillan et al. [46] used SPME for sedimenting fiber suspensions, simulating systems of up to 512 fibers. Recently, Marin et al. [30, Paper III] used SE for the same problem, simulating up to 3800 fibers while using a more accurate fiber discretization.

In Paper II we extend the spectral Ewald to work with the stresslet potential, and apply it for a suspension of sedimenting spheroid particles.

Chapter 5

Ewald decompositions

As we have seen in the previous chapter, Ewald summation is a very useful technique for summing periodic potentials which converge slowly, if at all, when summed directly. To apply the technique to a given potential, one first requires what is called an Ewald decomposition. The decomposition splits the potential into two parts, one which is short-ranged and converges rapidly in real space, and one which is smooth and converges rapidly in \mathbf{k} -space. As we shall see, decompositions are not unique, and there are several ways of constructing a decomposition of a given potential.

We will here describe two general approaches for creating decompositions, and relate them to each other in a way which we have not seen documented before. We will then show how this relation can be used to create new decompositions with relatively little effort.

5.1 Splitting and screening

Given a PDE in free space (with the Laplace equation as an example in parentheses),

$$Lu = 4\pi q\delta, \quad (L = -\Delta),$$

we have a Green's function s.t.

$$u = qG, \quad (G = \frac{1}{r}).$$

In many cases, the Green's function can also be expressed as an operation K on r ,

$$G = Kr, \quad (K = \frac{1}{2}\Delta). \tag{5.1}$$

In a periodic setting, u will be computed by summing all periodic images of G . If G decays slowly ($1/r$) an Ewald decomposition is required to compute the sum in a fast way. Such a decomposition can be obtained by splitting the operator K or by screening the Green's function G .

Splitting

The splitting method was invented by Beenakker [4] for the Rotne-Prager tensor, and later applied on the stokeslet by Pozrikidis [40], and on the stresslet by Fan & Phan-Thien [16]. The decomposition is obtained by introducing Φ and Θ , such that

$$\Phi + \Theta = r,$$

and writing

$$G^F + G^R = K(\Phi + \Theta).$$

The real space part is obtained by applying K to Θ , which in general is a matter of differentiation,

$$G^R = K \Theta,$$

while G^F is transformed to Fourier space,

$$\widehat{G}^F = \widehat{K} \widehat{\Phi},$$

where \widehat{K} is the transformed operator (Laplace: $\widehat{K} = -\frac{1}{2}k^2$). The Beenakker decomposition is obtained by setting

$$\begin{aligned} \Phi &= r \operatorname{erf}(\xi r), \\ \Theta &= r \operatorname{erfc}(\xi r), \end{aligned}$$

having (see [40])

$$\widehat{\Theta} = -\frac{8\pi}{k^4} \left(1 + \frac{1}{4} \frac{k^2}{\xi^2} + \frac{1}{8} \frac{k^4}{\xi^4} \right) e^{-k^2/4\xi^2}.$$

For the Laplace example, this yields

$$\begin{aligned} G^R &= \frac{1}{2} \Delta (r \operatorname{erf}(\xi r)) = \frac{\operatorname{erfc}(\xi r)}{r} + \frac{2\xi e^{-\xi^2 r^2} (\xi^2 r^2 - 2)}{\sqrt{\pi}}, \\ \widehat{G}^F &= -k^2 \mathcal{F}[r \operatorname{erfc}(\xi r)] = \frac{4\pi}{k^2} \left(1 + \frac{1}{4} \frac{k^2}{\xi^2} + \frac{1}{8} \frac{k^4}{\xi^4} \right) e^{-k^2/4\xi^2}. \end{aligned}$$

This particular decomposition is however of limited interest, since it is more complicated than the classical Ewald decomposition for the Laplacian, and is likely to have slower convergence. The point here is that it is very simple to apply the Beenakker method, given K in (5.1).

Screening

Screening is done by introducing a screening function γ , $\|\gamma(\mathbf{x})\| = 1$, that decays smoothly away from zero. The decomposition of G is then obtained by adding and subtracting the convolution of G and γ ,

$$G = G - (G * \gamma) + (G * \gamma),$$

such that

$$\begin{aligned} G^R &= G - (G * \gamma), \\ \widehat{G}^F &= \widehat{G}\widehat{\gamma}. \end{aligned}$$

The classical Ewald decomposition for Laplace uses

$$\gamma_E(\mathbf{x}) = \xi^3 \pi^{-3/2} e^{-\xi^2 r^2} \quad \Rightarrow \quad \widehat{\gamma}_E(\mathbf{k}) = e^{-k^2/4\xi^2},$$

which leads to the decomposition

$$\begin{aligned} G^R &= \frac{\operatorname{erfc}(\xi r)}{r} \\ \widehat{G}^F &= \frac{4\pi}{k^2} e^{-k^2/4\xi^2}. \end{aligned}$$

For the Stokeslet, the original derivation of the Ewald decomposition by Hasimoto [22] did not involve a screening function. However, it was later shown by Hernández-Ortiz et al. [23] that it is equivalent to applying the screening function

$$\gamma_H(\mathbf{x}) = \xi^3 \pi^{-3/2} e^{-\xi^2 r^2} \left(\frac{5}{2} - \xi^2 r^2 \right) \quad \Rightarrow \quad \widehat{\gamma}_H(\mathbf{k}) = e^{-k^2/4\xi^2} \left(1 + \frac{1}{4} \frac{k^2}{\xi^2} \right).$$

The screening method has one drawback, which is that evaluating the convolution ($G * \gamma$) can be quite tedious. Reproducing the result by Hernández-Ortiz et al. requires a fair amount of calculations.

Relationship between methods

Screening and splitting can be viewed as two different ways of obtaining the same decomposition. There is then a relationship between (Φ, Θ) and γ , which can be explicitly expressed as

$$\begin{aligned} \mathbf{K} \Theta &= G - (G * \gamma), \\ \widehat{\mathbf{K}} \widehat{\Phi} &= \widehat{G} \widehat{\gamma}. \end{aligned}$$

However, since $G = \mathbf{K} r$, we have the relationship

$$\widehat{G} = -\frac{8\pi}{k^4} \widehat{\mathbf{K}},$$

and so

$$\widehat{\Phi} = -\frac{8\pi}{k^4}\widehat{\gamma} \quad \Leftrightarrow \quad \widehat{\gamma} = -\frac{k^4}{8\pi}\widehat{\Phi}$$

and

$$\gamma = -\frac{1}{8\pi}\nabla^4\Phi. \quad (5.2)$$

Given a decomposition $r = \Phi + \Theta$, we can then calculate the corresponding screening function γ by simple differentiation of Φ . Conversely, assuming Φ spherically symmetric, we can get Φ for a given γ by solving the biharmonic equation (5.2) in spherical coordinates,

$$\frac{4}{r}\Phi^{(3)}(r) + \Phi^{(4)}(r) = -\frac{1}{8\pi}\gamma(r).$$

5.2 Summary of decompositions

We are now able to complete Tables 5.1 and 5.2, where we list screening functions and corresponding splitting for the Ewald, Hasimoto and Beenakker methods, some of which have not been previously published. This allows us a comprehensive view of the decomposition methods so far listed in the literature. It also provides us with shortcuts if we want to calculate either decomposition for a given potential. If we, for example, want to calculate the Hasimoto decomposition for a given G , we might be reluctant to carry out the calculation of $(G * \gamma_H)$. If we know K , we can instead get G^R directly by applying K to Φ , which in general is a much simpler operation.

Name	Screening function $\gamma(r)$	Fourier screening $\widehat{\gamma}(k)$
Ewald, γ_E	$\alpha e^{-\xi^2 r^2}$	$e^{-k^2/4\xi^2}$
Hasimoto, γ_H	$\alpha e^{-\xi^2 r^2} \left(\frac{5}{2} - \xi^2 r^2\right)$	$e^{-k^2/4\xi^2} \left(1 + \frac{1}{4} \frac{k^2}{\xi^2}\right)$
Beenakker, γ_B	$\alpha e^{-\xi^2 r^2} (10 - 11\xi^2 r^2 + 2\xi^4 r^4)$	$e^{-k^2/4\xi^2} \left(1 + \frac{1}{4} \frac{k^2}{\xi^2} + \frac{1}{8} \frac{k^4}{\xi^4}\right)$

Table 5.1: Screening functions, $\alpha = \xi^3 \pi^{-3/2}$.

Name	Splitting $\Phi(r)$	Splitting $\Theta(r) = r - \Phi(r)$
Ewald, (Φ_E, Θ_E)	$r \operatorname{erf}(\xi r) + \frac{r \operatorname{erf}(\xi r)}{2\xi^2 r^2} + \frac{e^{-\xi^2 r^2}}{\sqrt{\pi\xi}}$	$r \operatorname{erfc}(\xi r) - \frac{r \operatorname{erf}(\xi r)}{2\xi^2 r^2} - \frac{e^{-\xi^2 r^2}}{\sqrt{\pi\xi}}$
Hasimoto, (Φ_H, Θ_H)	$r \operatorname{erf}(\xi r) + \frac{e^{-\xi^2 r^2}}{\sqrt{\pi\xi}}$	$r \operatorname{erfc}(\xi r) - \frac{e^{-\xi^2 r^2}}{\sqrt{\pi\xi}}$
Beenakker, (Φ_B, Θ_B)	$r \operatorname{erf}(\xi r)$	$r \operatorname{erfc}(\xi r)$

Table 5.2: Splittings, $\Theta(r) + \Phi(r) = r$.

Chapter 6

Conclusions and future work

In this thesis we have discussed numerical methods related to two types of fluid flow which are of interest in microfluidics: multiphase flow and sedimentation in particle suspensions. In the two included papers (Paper I and Paper II) we present methods for simulating these respective flow types.

The method presented in Paper I can be used for simulating complex flows involving surfactants and moving contact lines. It is based on an interface tracking method where the interface is decomposed into segments. This provides a natural framework for the treatment of surfactants and contact lines, but is limited to two dimensions. Extending this method to three dimensions is not straightforward, as discussed in [26], and we have chosen not to continue along this path of development.

In Paper II we present our most recent work, which is a fast boundary integral method for periodic Stokes flow in three dimensions, applied to sedimentation in particle suspensions. Continuing the development of this method is our current focus, with the next step being to improve the quadrature used for the boundary integrals, such that very close interaction between particles can be treated with control of the numerical errors. Future work will be directed towards further development of the method, to allow for high accuracy quadrature over particles of general shape. Possible research then includes extending the method to handle deformable particles and interfaces between immiscible fluids.

Bibliography

- [1] S. Adami, X. Hu, and N. Adams. A conservative SPH method for surfactant dynamics. *J. Comput. Phys.*, 229(5):1909–1926, 2010, doi:10.1016/j.jcp.2009.11.015.
- [2] C. K. Aidun and J. R. Clausen. Lattice-Boltzmann Method for Complex Flows. *Annu. Rev. Fluid Mech.*, 42(1):439–472, 2010, doi:10.1146/annurev-fluid-121108-145519.
- [3] D. M. Anderson, G. B. McFadden, and A. A. Wheeler. Diffuse-Interface methods in Fluid Mechanics. *Annu. Rev. Fluid Mech.*, 30(1):139–165, 1998, doi:10.1146/annurev.fluid.30.1.139.
- [4] C. W. J. Beenakker. Ewald sum of the Rotne-Prager tensor. *The J. Chem. Phys.*, 85(3):1581, 1986, doi:10.1063/1.451199.
- [5] T. D. Blake. The physics of moving wetting lines. *J. Colloid. Interf. Sci.*, 299(1):1–13, 2006, doi:10.1016/j.jcis.2006.03.051.
- [6] D. Bonn, J. Eggers, J. Indekeu, J. Meunier, and E. Rolley. Wetting and spreading. *Rev. Mod. Phys.*, 81(2):739–805, 2009, doi:10.1103/RevModPhys.81.739.
- [7] M. Booty and M. Siegel. A hybrid numerical method for interfacial fluid flow with soluble surfactant. *J. Comput. Phys.*, 229(10):3864–3883, 2010, doi:10.1016/j.jcp.2010.01.032.
- [8] J. Brackbill, D. Kothe, and C. Zemach. A continuum method for modeling surface tension. *J. Comput. Phys.*, 100(2):335–354, 1992, doi:10.1016/0021-9991(92)90240-Y.
- [9] A. Carlson, M. Du-Quang, and G. Aamberg. Dissipation in rapid dynamic wetting. *J. Fluid Mech.*, 682:213–240, 2011, doi:10.1017/jfm.2011.211.
- [10] S. Chen and G. D. Doolen. Lattice Boltzmann method for fluid flows. *Annu. Rev. Fluid Mech.*, 30(1):329–364, 1998, doi:10.1146/annurev.fluid.30.1.329.
- [11] R. H. Davis and A. Acrivos. Sedimentation of Noncolloidal Particles at Low Reynolds Numbers. *Annu. Rev. Fluid Mech.*, 17(1):91–118, 1985, doi:10.1146/annurev.fl.17.010185.000515.

- [12] P. G. de Gennes. Wetting: statics and dynamics. *Rev. Mod. Phys.*, 57(3):827–863, 1985, doi:10.1103/RevModPhys.57.827.
- [13] J. W. Demmel. *Applied Numerical Linear Algebra*. Society for Industrial and Applied Mathematics, 1997, doi:10.1137/1.9781611971446.
- [14] M. Deserno and C. Holm. How to mesh up Ewald sums. I. A theoretical and numerical comparison of various particle mesh routines. *The J. Chem. Phys.*, 109(18):7678, 1998, doi:10.1063/1.477414.
- [15] P. P. Ewald. Die Berechnung optischer und elektrostatischer Gitterpotentiale. *Annalen der Physik*, 369(3):253–287, 1921, doi:10.1002/andp.19213690304.
- [16] X. Fan, N. Phan-Thien, and R. Zheng. Completed double layer boundary element method for periodic suspensions. *Z. angew. Math. Phys.* 49, 49(2):167, 1998, doi:10.1007/s000330050214.
- [17] S. Ganesan and L. Tobiska. A coupled arbitrary Lagrangian-Eulerian and Lagrangian method for computation of free surface flows with insoluble surfactants. *J. Comput. Phys.*, 228(8):2859–2873, 2009, doi:10.1016/j.jcp.2008.12.035.
- [18] O. Gonzalez. On Stable, Complete, and Singularity-Free Boundary Integral Formulations of Exterior Stokes Flow. *SIAM J. on Appl. Math.*, 69(4):933–958, 2009, doi:10.1137/070698154.
- [19] E. Guazzelli. Sedimentation of small particles: how can such a simple problem be so difficult? *C. R. Mecanique*, 334(8-9):539–544, 2006, doi:10.1016/j.crme.2006.07.009.
- [20] E. Guazzelli and J. Hinch. Fluctuations and Instability in Sedimentation. *Annu. Rev. Fluid Mech.*, 43(1):97–116, 2011, doi:10.1146/annurev-fluid-122109-160736.
- [21] K. Gustavsson and A.-K. Tornberg. Gravity induced sedimentation of slender fibers. *Phys. Fluids*, 21(12):123301, 2009, doi:10.1063/1.3273091.
- [22] H. Hasimoto. On the periodic fundamental solutions of the Stokes equations and their application to viscous flow past a cubic array of spheres. *J. Fluid Mech.*, 5(02):317, 1959, doi:10.1017/S0022112059000222.
- [23] J. Hernández-Ortiz, J. de Pablo, and M. Graham. Fast Computation of Many-Particle Hydrodynamic and Electrostatic Interactions in a Confined Geometry. *Phys. Rev. Lett.*, 98(14):140602, 2007, doi:10.1103/PhysRevLett.98.140602.
- [24] S. Khatri and A.-K. Tornberg. A numerical method for two phase flows with insoluble surfactants. *Comput. & Fluids*, 49(1):150–165, 2011, doi:10.1016/j.compfluid.2011.05.008.

- [25] J. Kolafa and J. W. Perram. Cutoff Errors in the Ewald Summation Formulae for Point Charge Systems. *Mol. Simul.*, 9(5):351–368, 1992, doi:10.1080/08927029208049126.
- [26] D. Lindbo. *Spectral Accuracy in Fast Ewald Methods and Topics in Fluid Interface Simulation*. Phd thesis, KTH, 2011, <http://urn.kb.se/resolve?urn=urn:nbn:se:kth:diva-48805>, .
- [27] D. Lindbo and A.-K. Tornberg. Spectrally accurate fast summation for periodic Stokes potentials. *J. Comput. Phys.*, 229(23):8994–9010, 2010, doi:10.1016/j.jcp.2010.08.026.
- [28] D. Lindbo and A.-K. Tornberg. Spectral accuracy in fast Ewald-based methods for particle simulations. *J. Comput. Phys.*, 230(24):8744–8761, 2011, doi:10.1016/j.jcp.2011.08.022.
- [29] H. Liu and Y. Zhang. Phase-field modeling droplet dynamics with soluble surfactants. *J. Comput. Phys.*, 229(24):9166–9187, 2010, doi:10.1016/j.jcp.2010.08.031.
- [30] O. Marin. *Boundary integral methods for Stokes flow : Quadrature techniques and fast Ewald methods*. PhD thesis, KTH Royal Institute of Technology, 2012, <http://urn.kb.se/resolve?urn=urn:nbn:se:kth:diva-105540>, .
- [31] M. Muradoglu and S. Tasoglu. A front-tracking method for computational modeling of impact and spreading of viscous droplets on solid walls. *Comput. & Fluids*, 39(4):615–625, 2010, doi:10.1016/j.compfluid.2009.10.009.
- [32] M. Muradoglu and G. Tryggvason. A front-tracking method for computation of interfacial flows with soluble surfactants. *J. Comput. Phys.*, 227(4):2238–2262, 2008.
- [33] P. Nithiarasu. An arbitrary Lagrangian Eulerian (ALE) formulation for free surface flows using the characteristic-based split (CBS) scheme. *Int. J. for Numer. Methods Fluids*, 48(12):1415–1428, 2005, doi:10.1002/fld.987.
- [34] E. Olsson and G. Kreiss. A conservative level set method for two phase flow. *J. Comput. Phys.*, 210(1):225–246, 2005.
- [35] Y. Pawar and K. J. Stebe. Marangoni effects on drop deformation in an extensional flow: The role of surfactant physical chemistry. I. Insoluble surfactants. *Phys. Fluids*, 8(7):1738, 1996, doi:10.1063/1.868958.
- [36] C. S. Peskin. Numerical-analysis of blood-flow in heart. *J. Comput. Phys.*, 25:220–252, 1977.
- [37] C. S. Peskin. The immersed boundary method. *Acta Numer.*, 11(-1):479–517, 2002.

- [38] H. Power and G. Miranda. Second Kind Integral Equation Formulation of Stokes Flows Past a Particle of Arbitrary Shape. *SIAM J. on Appl. Math.*, 47(4):689, 1987, doi:10.1137/0147047.
- [39] C. Pozrikidis. *Boundary Integral and Singularity Methods for Linearized Viscous Flow*. Cambridge University Press, Cambridge, 1992, doi:10.1017/CBO9780511624124.
- [40] C. Pozrikidis. Computation of periodic Green's functions of Stokes flow. *J. Eng. Math.*, 30(1-2):79–96, 1996, doi:10.1007/BF00118824.
- [41] E. M. Purcell. Life at low Reynolds number. *Am. J. Phys.*, 45(1):3, 1977, doi:10.1119/1.10903.
- [42] S. Quan, J. Lou, and D. P. Schmidt. Modeling merging and breakup in the moving mesh interface tracking method for multiphase flow simulations. *J. Comput. Phys.*, 228(7):2660–2675, 2009, doi:10.1016/j.jcp.2008.12.029.
- [43] S. Quan and D. P. Schmidt. A moving mesh interface tracking method for 3D incompressible two-phase flows. *J. Comput. Phys.*, 221(2):761–780, 2007, doi:10.1016/j.jcp.2006.06.044.
- [44] W. Ren and W. E. Boundary conditions for the moving contact line problem. *Phys. Fluids*, 19(2):22101, 2007, doi:10.1063/1.2646754.
- [45] Y. Saad and M. H. Schultz. GMRES: A Generalized Minimal Residual Algorithm for Solving Nonsymmetric Linear Systems. *SIAM J. on Sci. Stat. Comput.*, 7(3):856–869, 1986, doi:10.1137/0907058.
- [46] D. Saintillan, E. Darve, and E. S. G. Shaqfeh. A smooth particle-mesh Ewald algorithm for Stokes suspension simulations: The sedimentation of fibers. *Phys. Fluids*, 17(3):033301, 2005, doi:10.1063/1.1862262.
- [47] R. Scardovelli and S. Zaleski. Direct numerical simulation of free-surface and interfacial flow. *Annu. Rev. Fluid Mech.*, 31:567–603, 1999.
- [48] J. A. Sethian and P. Smereka. Level set methods for fluid interfaces. *Annu. Rev. Fluid Mech.*, 35:341–372, 2003, doi:10.1146/annurev.fluid.35.101101.161105.
- [49] A. Sierou and J. F. Brady. Accelerated Stokesian Dynamics simulations. *J. Fluid Mech.*, 448:115–146, 2001, doi:10.1017/S0022112001005912.
- [50] H. A. Stone. A simple derivation of the time-dependent convective-diffusion equation for surfactant transport along a deforming interface. *Phys. Fluids A: Fluid Dyn.*, 2(1):111, 1990, doi:10.1063/1.857686.
- [51] H. A. Stone. Dynamics of Drop Deformation and Breakup in Viscous Fluids. *Annu. Rev. Fluid Mech.*, 26(1):65–102, 1994, doi:10.1146/annurev.fl.26.010194.000433.

- [52] H. A. Stone, A. D. Stroock, and A. Ajdari. Engineering flows in small devices: Microfluidics toward a lab-on-a-chip. *Annu. Rev. Fluid Mech.*, 36:381–411, 2004, doi:10.1146/annurev.fluid.36.050802.122124.
- [53] P. Tabeling. *Introduction to microfluidics*. Oxford University Press, USA, 2005.
- [54] S. Takagi and Y. Matsumoto. Surfactant Effects on Bubble Motion and Bubbly Flows. *Annu. Rev. Fluid Mech.*, 43(1):615–636, 2011, doi:10.1146/annurev-fluid-122109-160756.
- [55] K. E. Teigen, P. Song, J. Lowengrub, and A. Voigt. A diffuse-interface method for two-phase flows with soluble surfactants. *J. computational physics*, 230(2):375–393, 2011, doi:10.1016/j.jcp.2010.09.020.
- [56] G. Tryggvason, B. Bunner, A. Esmaeli, D. Juric, N. Al-Rawahi, W. Tauber, J. Han, S. Nas, and Y. J. Jan. A front-tracking method for the computations of multiphase flow. *J. Comput. Phys.*, 169:708–759, 2001.
- [57] S. O. Unverdi and G. Tryggvason. A front-tracking method for viscous, incompressible, multi-fluid flows. *J. Comput. Phys.*, 100(1):25–37, 1992, doi:10.1016/0021-9991(92)90307-K.
- [58] M. Wörner. Numerical modeling of multiphase flows in microfluidics and micro process engineering: a review of methods and applications. *Microfluid. Nanofluidics*, 12(6):841–886, 2012, doi:10.1007/s10404-012-0940-8.
- [59] S. Wrobel. Bubbles, Babies and Biology: The Story of Surfactant. *The FASEB J.*, 18(13):1624e–1624e, 2004, doi:10.1096/fj.04-2077bkt.
- [60] J.-J. Xu, Y. Yang, and J. Lowengrub. A level-set continuum method for two-phase flows with insoluble surfactant. *J. Comput. Phys.*, 231(17):5897–5909, 2012, doi:10.1016/j.jcp.2012.05.014.
- [61] S. Zahedi, K. Gustavsson, and G. Kreiss. A conservative level set method for contact line dynamics. *J. Comput. Phys.*, 228(17):6361–6375, 2009, doi:10.1016/j.jcp.2009.05.043.
- [62] C.-X. Zhao and A. P. Middelberg. Two-phase microfluidic flows. *Chem. Eng. Sci.*, 66(7):1394–1411, 2011, doi:10.1016/j.ces.2010.08.038.